Tissue Barriers 3:4, e1105907; October/November/December 2015; © 2015 Taylor & Francis Group, LLC

A proposed route to independent measurements of tight junction conductance at discrete cell junctions

Lushan Zhou[1], Yuhan Zeng[1], Lane A Baker[1,*], and Jianghui Hou[2,3,*]

[1]Department of Chemistry; Indiana University; Bloomington, IN USA; [2]Department of Internal Medicine - Renal Division; St. Louis, MO USA; [3]Center for Investigation of Membrane Excitability Diseases; Washington University Medical School; St. Louis, MO USA

Keywords: conductance, ion channel, patch clamp, SICM, tight junction

Abbreviations: *a*, nanopore inner radius (eqn. 2-3); BE, balance electrode; CE, counter electrode; C_{ma}, apical membrane capacitance; C_{mb}, basolateral membrane capacitance; C_S, capacitance of patch clamp pipet; *d*, nanopore diameter (**Fig. 4B** caption); D_{ps}, probe-surface distance; DVC-ICM, double whole-cell voltage clamp ion conductance microscopy; E, electric field (eqn.1); E_{rest}, resting membrane potential; G, conductance (eqn.1); GND, electrical ground; *h*, cylindrical nanopore length (**Fig. 4B** caption); *I*, current across C_{mb1} (eqn. 5-6); i.d., inner radius; i_{BE}, balance electrode current; i_{GJ}, gap junctional current; i_{ma}, apical membrane current; i_{mb}, basolateral membrane current; i_{para}, paracellular current; i_{trans}, transcellular current; JAMs, Junctional Adhesion Molecules; MDCK, Madin-Darby canine kidney; PE, pipet electrode; P-SICM, potentiometric scanning ion conductance microscopy; *r*, distance from the axis of symmetry (eqn.3); RC, resistor capacitor circuit or product of resistance and capacitance; RE, reference electrode; R_{GJ}, gap junction resistance; R_L, leak resistance (or seal resistance); R_{ma}, apical membrane resistance; R_{mb}, basolateral membrane resistance; R_{pore}, nanopore resistance (**Fig. 4B** caption); R_S, series resistance; R_{TE}, transepithelial resistance; R_{TJ}, tight junction resistance; S/N, signal-to-noise ratio; SICM, scanning ion conductance microscopy; TEER, transepithelial electrical resistance; TJs, tight junctions; UE, potential electrode; V, command voltage at balance electrode; V', actual intracellular potential (holding potential); V_{TE}, transepithelial potential; WE, working electrode; ΔV, potential deflection (eqn.1); *z*, normal distance from the pore (eqn.2-4); Δz, pipet vertical displacement (eqn. 1); ξ, η, rotational elliptic coordinates (eqn. 2-4); ρ, specific resistance of bath electrolyte (eqn. 1 **Fig. 4B**); Φ, potential at a certain position above nanopore (eqn. 4); Φ_0, potential at the nanopore surface (eqn.4)

Direct recording of tight junction permeability is of pivotal importance to many biologic fields. Previous approaches bear an intrinsic disadvantage due to the difficulty of separating tight junction conductance from nearby membrane conductance. Here, we propose the design of Double whole-cell Voltage Clamp - Ion Conductance Microscopy (DVC-ICM) based on previously demonstrated potentiometric scanning of local conductive pathways. As proposed, DVC-ICM utilizes two coordinated whole-cell patch-clamps to neutralize the apical membrane current during potentiometric scanning, which in models described here will profoundly enhance the specificity of tight junction recording. Several potential pitfalls are considered, evaluated and addressed with alternative countermeasures.

Tight Junctions

Tight junctions (TJs) form a continuous paracellular seal between adjacent epithelial cells and control solute transport between apical and basolateral fluids. In thin section electron microscopy, TJs appear as series of direct membrane contacts, where membranes from adjacent cells fuse together,[1] and freeze-fracture electron microscopy has further revealed TJs to exist as extended protein strands that form transmembrane networks.[2] Known integral membrane proteins of the tight junction include occludin,[3] Junctional Adhesion Molecules (JAMs),[4] and claudins.[5] Claudins have been shown to confer ion selectivity to tight junctions. For instance, claudin-4, -5, -8, -11 and -14 selectively decrease cation permeability,[6-10] whereas claudin-15 and -17 are anion selective.[11,12] Permeability studies suggest paracellular channels 4-7 Å in diameter are formed from claudins at tight junction contacts and are responsible for the selectivity in ion transport.[13,14] The first crystal structure of claudin has recently been published,[15] which primes the field to study the structure and function relationship of tight junction. The present study offers a new approach for assessing the conductive properties of tight junction with unprecedented resolution.

*Correspondence to: Lane A Baker; Email: lanbaker@indiana.edu; Jianghui Hou; Email: jhou@wustl.edu
Submitted: 08/24/2015; Revised: 10/01/2015; Accepted: 10/05/2015
http://dx.doi.org/10.1080/21688370.2015.1105907

Measurement of Tight Junction Conductance

Tight junction permeability is often experimentally assessed by electrical measurements of transepithelial ion transport. For instance, in the classic Ussing chamber,[16-20] the transepithelial electrical resistance (TEER) is measured to determine the transepithelial resistance (R_{TE}, inverse of epithelial conductance) of tissue slices and the dilution potential is recorded to determine the ion selectivity of the conductive pathways. This approach can also be translated to cells cultured on polymer membranes, where hundreds to thousands of cells can be measured in a single TEER measurement, with R_{TE} values recorded that are typically in the range of 10-1000s of $\Omega \cdot cm^2$. Although useful, TEER measurements represent the aggregate response of all ion-conductive pathways, which include transcellular ion channels as well as paracellular channels. Approaches to separate the two conductivity pathways (transcellular, paracellular) are difficult to achieve experimentally. Two-path impedance spectroscopy[21] has been perhaps most successful in distinguishing between paracellular and transcellular conductances, but still lacks local information for studying heterogeneously conductive epithelium. In particular, delineation of paracellular conductance from an epithelium proves especially challenging. If we consider patch-clamp techniques[22] as the "gold standard" to measure ion transport of protein channels in the transcellular pathway, no comparable approach exists to study components of paracellular conductance. Patch–clamp approaches appear unsuitable for direct measurement of tight junctions because of the inability to form gigaohm seals between pipet and the cell perimeter where the tight junction resides.

Frömter and co-workers pioneered a little used, but particularly intriguing method to separate paracellular and transcellular conductances through voltage scanning (or conductance scanning) technique, in which local voltage deflections over individual cell junctions are measured.[23,24] Voltage scanning makes use of a pair of microelectrodes that are positioned in space above a cell or tissue monolayer. With application of a pulsed current across the epithelial cell layer, the microelectrodes can be used to record spatially resolved conductance. However, limitations of this technique exist due to lack of accurate electrode position control and low signal-to-noise ratios (S/N), making voltage scanning only applicable to very flat epithelia and cases where tight junction conductance differs significantly from the transcellular conductance. We have adapted the general conductance scanning concepts of Frömter into scanning ion conductance microscopy (SICM)[25] with a goal of improving resolution through better probe control and experimental flexibility. SICM utilizes an ion conductance feedback mechanism to scan an electrolyte filled nanopipet over a surface. SICM provides relatively high-resolution surface topography (<100 nm), which is then used to position the nanopipet probe accurately over cell-cell junctions. Additionally, the robust feedback control of SICM allows precise control of probe-cell surface distance (at the nanometer scale) during measurement and not only flat but also rough epithelial surfaces to be studied. To record tight junction conductance with SICM, the nanopipet is positioned over a tight junction and local ion current is recorded as a transepithelial potential is applied across the epithelium. To compensate for limits in S/N in the current-based measurement due to the high resistance of the probe, we introduce an additional electrode that measures the potential at the pipet tip, in an SICM mode we termed potentiometric scanning ion conductance microscopy (P-SICM).[26]

Potentiometric Scanning Ion Conductance Microscopy (P-SICM)

P-SICM utilizes a dual barrel nanopipet to scan and measure epithelial cell layers grown on a filter mounted between 2 chambers of a perfusion well (**Fig. 1**). The tip diameter of each barrel of the pipet typically ranges from 10 - 100 nanometers, as determined with scanning electron micrographs. The pipet electrode (PE, biased at 100 mV vs. reference electrode (RE)) present in one barrel monitors the probe-surface distance (D_{ps}) dependent ion current to control probe position. A potential electrode (UE) in the second barrel measures the local potential deflection (also with respect to RE). A platinum counter electrode (CE) drives the majority of transepithelial current to avoid potential fluctuations of RE when a transepithelial potential (V_{TE}) is applied at the working electrode (WE) placed in the bottom chamber. V_{TE} drives ion current through cell-cell junctions as well as membrane channels and results in a potential gradient in the vicinity of these ion conductive pathways. Local potential variations captured by UE can then be used to determine apparent local conductance (G) values from **Equation 1**.[27,28]

$$G = \left(\frac{E}{\rho \cdot V_{TE}}\right) = \left(\frac{(\Delta V_{0.2\mu m} - \Delta V_{12.5\mu m})/\Delta z}{\rho \cdot V_{TE}}\right) \qquad (1)$$

In this equation, E represents the electric field (potential gradient) induced by transepithelial potential V_{TE} and ρ is the specific resistance of the bath electrolyte. In P-SICM measurements, UE records local potentials at two D_{ps} (typically 0.2 μm and 12.5 μm above the cell junction or cell body), which are then used to calculate the electric field, knowing the pipet vertical displacement ($\Delta z = 0.2$ μm to 12.5 μm). To avoid polarization of the cell plasma membrane, an alternating transepithelial potential (V_{TE}) is utilized, at a frequency (typically 1 Hz) selected to minimize capacitive contributions. The magnitude of V_{TE} is usually held to less than 50 mV to avoid cell damage and disruption of the cell membrane.[29,30]

We have previously shown that P-SICM results in significantly enhanced S/N of approximately an order of magnitude for potential measurement (compared to current measurement).[26,31] We have also demonstrated P-SICM as a sensitive tool to distinguish small differences in paracellular and transcellular conductance in cell monolayers and proposed that P-SICM can be utilized in leaky epithelia that cannot be measured by other techniques.

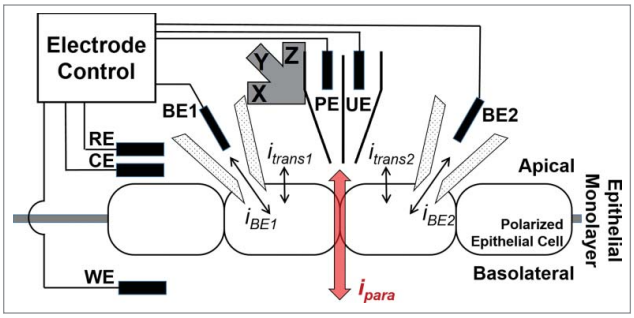

Figure 1. Illustration of the DVC-ICM setup. Double barrel pipet for topographical mapping (PE) and local potential measurement (UE) is attached to a piezo positioner. Reference electrode (RE), counter electrode (CE) and working electrode (WE) are controlled with home-built electrode controller to apply transmembrane potential across the epithelial monolayer. Two balance electrodes (BE1 and BE2) are used to control the intracellular potentials of 2 patched cells and to record the current flowing from or to BE1 or BE2 (i_{BE1} or i_{BE2}) respectively. Upon the application of transmembrane potential, ion current flows across the epithelial cell layer through both paracellular pathways (i_{para}) and transcellular pathways (i_{trans1} and i_{trans2}), and both i_{trans} are undesired background signal for the measurement of paracellular conductance.

Double Whole-cell Voltage Clamp Ion Conductance Microscopy (DVC-ICM)

Despite advantages in tight junction recordings with P-SICM, the multitude of competing conductance pathways and the use of a nonzero probe-surface distance (D_{ps}) may result in systematic errors that arise from transcellular conductance artifacts. To be specific, in the P-SICM configuration, the application of transepithelial potential (V_{TE}) drives ions to move across the cell layer through both paracellular (cell junctions) and transcellular (membrane ion channels) pathways. The resultant currents are indicated as i_{para} and i_{trans} in **Figure 1**. An unknown fraction of i_{trans} (mainly from the two cells forming the cell junction under study) will inevitably be picked up by the pipet (or from the potential gradient point of view, i_{trans} can interfere with local gradients at cell-cell junctions), especially at a D_{ps} of ~12.5 μm, where background conductance is measured (**Equation 1**). To more accurately record tight junction conductance, the background signal - i_{trans} from neighboring cells, has to be subtracted either through pharmacologic inhibition or mathematical deduction. However, pharmacologic inhibition would likely affect natural physiological processes, while the exact contribution from transcellular transport within neighboring cells of the measured tight junction needs to be known for the mathematical deduction approach, which turns out to be very difficult.

Here, we propose a new method to electrically offset contributions of i_{trans} from neighboring cells by coupling double whole-cell patch-clamps (commonly referred to as a double whole-cell patch-clamp)[32,33] with P-SICM measurements. The general idea of this method is to "zero out" the driving force for i_{trans} (due to the application of V_{TE}) by controlling the intracellular potential (membrane potential) of cells on either side of the tight junction with whole-cell patch-clamps. One reasonable assumption of this method is that i_{trans} from the two adjoining cells making the tight junction contribute to the major background signal in the previous P-SICM measurements at cell-cell junction compared to other cells that are further away from the junction (see detailed discussion below in "practical concerns" section).

Instrumentation

Figure 1 illustrates adaptation of the P-SICM instrumentation we have previously developed[26,31] to incorporate the double whole-cell patch-clamp. As in the previous P-SICM configuration, a double barrel pipet controls the probe position through the pipet electrode (PE) and measures local potential deflection at the potential electrode (UE). V_{TE} is applied to working electrode (WE) located on the basolateral side of the cell layer and a counter electrode (CE) close to the reference electrode (RE) drives the majority of the bulk ion current. The major instrumental advance is the addition of two micropipets that are patched to the two adjacent cells forming the cell junction being measured with P-SICM. We term these patched electrodes as "balance electrodes" (BEs). Each BE is controlled with a patch-clamp amplifier operating in voltage-clamp mode. During measurement, BE holds the intracellular potential at the resting membrane potential (E_{rest}) by providing a counter current (i_{BE}) through BE to eliminate the changes in intracellular potential due to the application of V_{TE}.

Equivalent circuit analysis

The origin of i_{trans} is the V_{TE} driven ion movement, which disrupts the natural resting membrane potential, which maintains a net i_{trans} of zero (although cellular processes generate a nonzero flux of specific ions). Therefore, the effect of V_{TE} on cell membranes must be "zeroed out" to eliminate the i_{trans} signal. To achieve this, DVC-ICM will clamp the membrane potential at E_{rest} value during the application of V_{TE}.

Figure 2A shows a proposed equivalent electric circuit for the DVC-ICM. Cell 1 and cell 2 are two adjoining cells that form a tight junction. At the cell junction, paracellular ion transport that occurs perpendicular to the epithelial cell layer is mediated through the tight junction, and the resistance of the TJ is represented as R_{TJ}. Gap junctions are also located in the cell junction and provide the primary path for ion transport between 2 cells. The resistance of the gap junction is R_{GJ}. For the cells, resistance of the apical membrane is indicated with R_{maj} (j=1 or 2, refers to cell 1 and cell 2 respectively) and resistance of the basolateral membrane is indicated by R_{mbj} (j=1 or 2). For each patch pipet, a series resistance R_{Sj} (j=1 or 2), which consists of the resistances of BE and the broken membrane patch, exists. Depending on the pipet geometry and electrolyte conductivity, R_S is typically on the order of 1-10 MΩ and draws a non-negligible voltage drop when current is passed through the patch pipet. The voltage drop across R_S causes V_j' (j=1 or 2), the actual intracellular potential or so-called holding potential, to differ from the command voltage at BE (V_1 and V_2 in **Figure 2A**). Current flowing through each resistor is labeled with the same subscript as shown in **Figure 2B**.

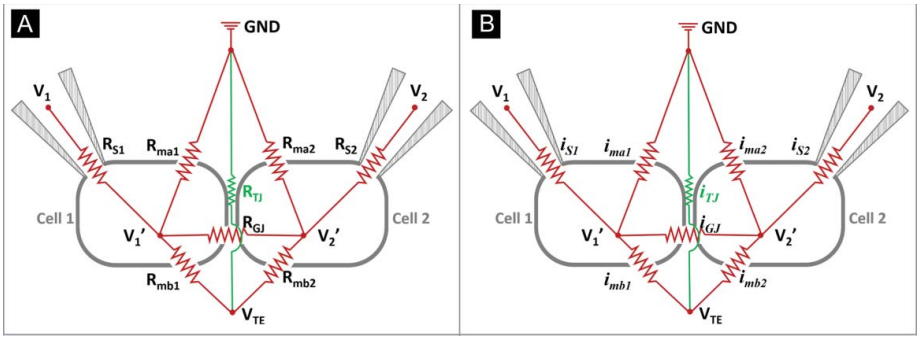

Figure 2. (**A**) Equivalent circuit of the DVC-ICM system. Here, tight junction conductance (reciprocal of tight junction resistance, R_{TJ}) of the junction formed by cell 1 and cell 2 is being measured with P-SICM (electrodes not shown). Cell 1 and cell 2 are voltage-clamped with two patch clamp pipets controlled with an individual patch clamp amplifier respectively. The intracellular potential of cell 1 (cell 2) is held at V_1' through BE1 (BE2), where the holding voltage by patch clamp amplifier is V_1 (V_2). Series resistance R_{S1} (R_{S2}) consists the resistances of BE and broken membrane patch from cell 1 (cell 2). Apical membrane resistance and basolateral membrane resistance are indicated separately with R_{ma1} and R_{mb1} for cell 1 and R_{ma2} and R_{mb2} for cell 2. R_{GJ} refers to the gap junction resistance through which ion current can pass between cell 1 and 2. (**B**) Ion current passing each resistor in (**A**) is labeled with the same subscript.

To simplify the circuit, R_{GJ} is omitted from the discussion, because the intracellular potential of cell 1 is considered to be equal to that of cell 2 in a uniform epithelial cell layer. Furthermore, the effects on the intracellular potentials of both cells from V_{TE} should be equivalent if 2 cells are considered "*electrically*" the same (gap junctional reversal potential is not considered here). Therefore $i_{GJ} = 0$ always holds, which means R_{GJ} can be considered an open circuit, and can be neglected in further circuit analysis.

With no external driving force - V_{TE}, the balance electrode potentials at patch pipets (V_1 and V_2) and the intracellular potentials remain at resting membrane potential value (E_{rest}, ~ −70 mV) and the net ion currents across cell membranes (i_{ma1}, i_{ma2}, i_{mb1}, i_{mb2}) are zero. In this circuit, with the application of V_{TE}, ion movement will take place either through the paracellular pathway (R_{TJ}) or the transcellular pathway (R_{mb1}+ R_{ma1}, and R_{mb2}+ R_{ma2}). The value of V_1' (or V_2') will deviate from E_{rest} due to the non-zero i_{mb1} (or i_{mb2}) driven by V_{TE}, and result in transmembrane current at the apical membrane side (i_{ma1} and i_{ma2}). This is the case for previous conductance scanning and P-SICM measurements. In the DVC-ICM configuration, the two patch pipets inject compensating currents through the BEs to clamp V_1' and V_2' at E_{rest} in the voltage clamp feedback loop of the patch clamp amplifiers. Since $V_1' = V_2' = E_{rest}$, the driving force for i_{ma1} and i_{ma2} due to the application of V_{TE} is eliminated and hence $i_{ma1} = i_{ma2} = 0$. Under this condition, the P-SICM probe positioned over this "electrically isolated" cell-cell junction will only measure the signal generated from the paracellular conductive pathway. Another way of analyzing current flow in the circuit is shown in **Figure 3**. The two BEs that provide compensation current can be viewed as much less resistive pathways in the circuit, which serves to shunt the majority of current flow (compared to the apical membranes) coming from the basolateral membrane.

Practical Concerns

Effects from neighboring cell-cell junctions

In the equivalent circuit shown in **Figure 2A**, only the resistance of the measured cell junction and the membrane resistance for 2 cells (cell 1 and cell 2) involved in forming this junction are considered. In a confluent epithelial cell layer, neighboring cells that are coupled to cell 1 and cell 2 by gap junctions will inevitably induce current flow to or from these 2 cells (**Fig. 4A**, green arrows). Additionally, the paracellular current at cell-cell junctions formed by cell 1 (or cell 2) with the neighboring cells (**Fig. 4A**, red arrows) may also be picked up by the P-SICM UE and hence contribute to background noise and unwanted signal for P-SICM measurements. Influence from these 2 effects is discussed here.

During P-SICM measurement, when a transepithelial potential (V_{TE}) is applied to the working electrode (WE, placed in the bottom chamber of the perfusion well) the intracellular potential for all cells in the epithelial layer will be altered by V_{TE}. In the proposed DVC-ICM model, only the two cells forming the junction under study are voltage-clamped at E_{rest}, which results in a difference in intracellular potential between either of the clamped cells (central green cells in **Figure 4A**, V_1' or V_2' in **Figure 2A**) and their closest neighbors (gray cells in the periphery in **Figure 4A**). Such intracellular potential differences may induce current flow through gap junctions (indicated with light green

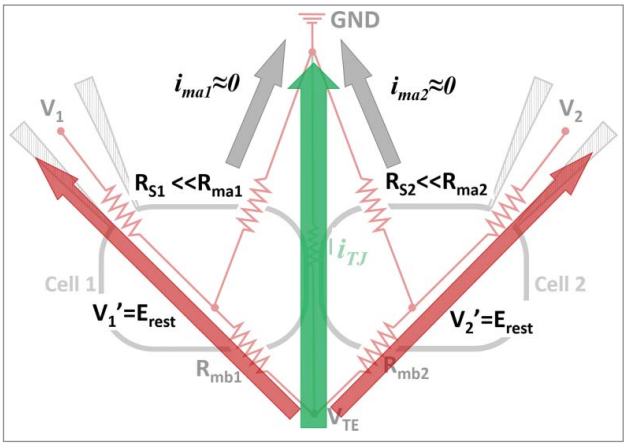

Figure 3. Intracellular potentials (V_1' and V_2') for both cell 1 and cell 2 are held at their E_{rest} to yield zero transmembrane current at the apical membranes (i_{ma1} and i_{ma2}) during the application of transmembrane potential V_{TE}. Majority of V_{TE} induced basolateral membrane current (i_{mb1} and i_{mb2}) is drawn through BE1 and BE2 (red arrows). Note: R_{GJ} is omitted from this circuit because V_1' and V_2' are always kept the same and there is no current through R_{GJ}.

arrows around the 2 central cells in **Figure 4A**), which may interrupt V_1' or V_2' in a manner similar to i_{mb1} or i_{mb2} discussed above. Nevertheless, these effects will be detected and compensated by the patch clamp amplifiers connected to the BEs. In other words, the BEs will eventually offset additional gap junctional current flow between cell 1 and cell 2, as V_1' and V_2' are always held at E_{rest}. Therefore, the gap junction current through neighboring cells will not contribute to i_{trans} in the proposed DVC-ICM model. The junctional reversal potential due to any type of asymmetry (e.g., voltage gating property of connexins) is not considered here but may also be eliminated by clamping $V_1'=V_2'$ at E_{rest}.

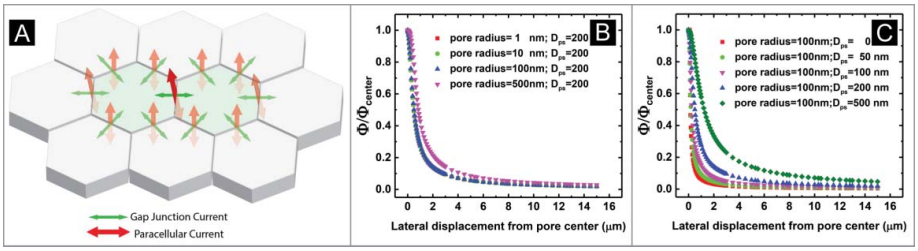

Figure 4. (**A**) Illustration of possible current flow between the two cells involved in DVC-ICM measurements (green cells in the middle) and their neighboring cells (gray cells in the periphery). Gap junctional currents flow within the epithelial cell layer (green arrow) and paracellular currents flow through tight junctions perpendicular to the cell layer (red arrow). (**B**) Lateral distribution of relative potential field (normalized to the potential amplitude over nanopore center) at 200 nm above a nanopore for nanopores with inner radius of 1, 10, 100 and 500 nm. The pore resistance (R_{pore}) of a cylindrical nanopore can be calculated by the following equation: $R_{pore} = p \cdot \frac{4h}{\pi \cdot d^2}$, in which *p* represents the solution resistivity, *d* represents the pore diameter, and *h* represents the pore length. (**C**) Lateral distribution of relative potential field (same as in (**B**)) at different heights above a radius 100 nm nanopore (D_{ps} = 0, 20, 100, 200, and 500 nm).

Another possible effect arises from the paracellular ion current at tight junctions formed by either cell 1 or cell 2 with other cells adjacent to them. These paracellular currents are indicated with light red arrows (vs. the dark red arrow at the cell 1-cell 2 junction) oriented perpendicular to the epithelial layer in **Figure 4A**. Although the paracellular channel density may vary at different cell-cell junctions to result in intrinsic variation of the measured conductance, the signals from neighboring junctions would have to be estimated and minimized to make the recording as accurate and localized as possible. First, UE is held over the center of a bicellular cell junction ("vs". the edge or corner of junctions) where the lateral distance between UE and the closest neighboring cell junctions is the largest (e.g., ~5-10 μm for epithelial cells such as MDCK). To estimate the relative potential field strength 5-10 μm away from versus at the field center (in this case, the tight junction), a previous mathematical model for calculation of potential distribution above a disk electrode is used.[34] Here, the tight junction channel at one individual cell-cell junction is treated as ideal nanopore geometry for simplicity. In this model, rotational elliptic coordinates ξ, η and *a* (nanopore inner radius) are used to express *z* (the normal distance from the pore) and *r* (distance from the axis of symmetry) as shown in **Equations (2-3)**.

$$z = a\xi\eta \tag{2}$$

$$r = a\sqrt{(1+\xi^2)(1-\eta^2)} \tag{3}$$

The potential Φ at a certain position can be determined as a function of ξ (**Equation 4**, Φ_0 is the potential at the nanopore surface).

$$\frac{\Phi}{\Phi_0} = 1 - \frac{2}{\pi}\tan^{-1}\xi \tag{4}$$

Figure 4B shows the relative potential distribution (normalized to the potential value above nanopore center) at D_{ps} of 200 nm above the surface for different sized nanopores (pore radii are 1, 10, 100, 500 nm). Generally, the shape of the curve is not influenced by nanopore radius and the potential drops rapidly (by ~90%) through distances within 2 μm from the nanopore center. At 5-10 μm from the pore center, the potential gradient changes very little and is approximately equal to the baseline value for the potential measured at a farther away distance (D_{ps} = 12.5 μm, simulation results not shown). Thus, at scales and potentials described here, we expect that contributions from nearby cell-cell junctions can be negligible. Controlling D_{ps} provides an additional route to minimize the signal from neighboring cell-cell junctions. As shown in **Figure 4C**, as D_{ps} decreases, the potential gradient above a 100 nm radius pore becomes sharper and results in a much more localized potential field.

Voltage-Gated Membrane Channels

Voltage-gated membrane channels are transmembrane ion channels that allow ion transport in response to changes in the membrane potential.[35-37] In P-SICM, V_{TE} is typically swept from -50 mV to +50 mV at 1 Hz. From previous studies, this potential range (at least at +50 mV) is sufficient to excite many types of voltage-gated channels, which will also contribute to i_{trans}. Because 1 Hz (the frequency V_{TE} is swept at) is much slower than the frequency needed to activate voltage-gated channels,[38] clamping the cell intracellular potentials at resting membrane potential (E_{rest}) can effectively avoid activation of voltage-gated membrane channels in the apical membrane and hence minimize the i_{trans} from these channels.

How Effectively can V1′ and V2′ be Clamped?

The equivalent electric circuit in **Figure 2A** includes key resistance components in the DVC-ICM system, other resistors and capacitors are added in **Figure 5** and need to be considered to evaluate the accuracy and response speed in clamping the intracellular potentials of the two cells (V_1' and V_2').

First, the voltage drop across R_{S1} (or R_{S2}) due to current flow through BE causes a difference between V_1 (or V_2), the amplifier command voltage, and V_1' (or V_2'), the actual intracellular

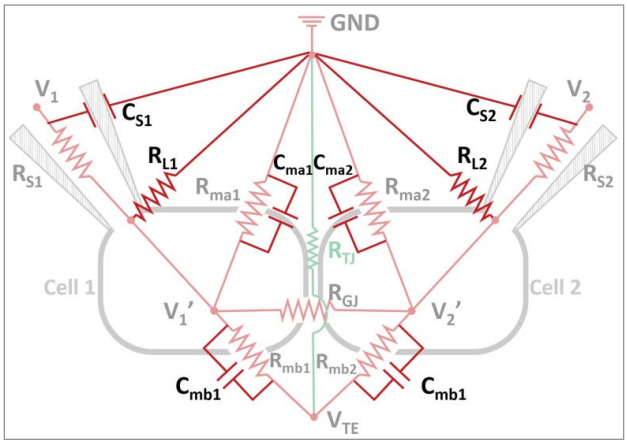

Figure 5. A more complete equivalent circuit of DVC-ICM system. C_{S1} and C_{S2} represent the capacitance of the patch clamp pipets glass wall. R_{L1} and R_{L2} are the "gigaohm seal" resistances at the sealed spaces between patch pipets and cell membranes. The cell membrane capacitances are indicated with C_{ma1}, C_{ma2} (for apical membrane) and C_{mb1}, C_{mb2} (for basolateral membrane).

potential. This effect becomes more significant when R_{S1} (or R_{S2}) is larger and cell membrane resistance becomes smaller. For instance, typical values for R_{S1} (or R_{S2}) are on the order of 1-10 MΩ, and the cell membrane resistance can range from GΩ[39] to tens of MΩ,[40-42] dependent on the cell type. One way to accurately hold V_1' (or V_2') at E_{rest} is to set the value of V_1 (or V_2) as the sum of E_{rest} and the voltage drop across BE. To do this, the value of R_{S1} (or R_{S2}) and the BE current need to be known. Ion current at each BE is constantly monitored under V-clamp mode by the patch clamp amplifiers, while R_{S1} (or R_{S2}) can be obtained by application of a test pulse of known amplitude between BE and RE (GND in **Figure 5**) and measurement of the corresponding current before and after formation of the gigaohm seal.

Second, in principle, the resistance of the sealed space (between pipet tip and cell membrane) should be infinite to guarantee no leakage current from the seal. In practice, however, the seal resistance (or leak resistance as R_{L1} and R_{L2} in **Figure 5**) is on the order of GΩ or hundreds of MΩ for a poor seal. R_{L1} and R_{L2} are in parallel with cell membrane resistances as shown in circuit in **Figure 5**. For highly resistive cell membranes, the seal resistances become comparable to membrane resistances and may need to be considered when setting the holding potential values. R_{L1} and R_{L2} can be measured in a manner similar to that described for R_{S1} and R_{S2} through the application of a test pulse.

Third, the RC response of the system, or the speed at which potentials are built up in the equivalent circuit should be evaluated. For example in cell 1, the changes in V_{TE} induce changes in V_1', which is clamped by V_1 through the patch pipet R_{S1}. As shown in **Figure 5**, circuit components involved in this current path include V_1, R_{S1}, V_1', R_{mb1}, C_{mb1} and V_{TE} (capacitances for Ag/AgCl BEs are omitted because capacitive charging current is negligible for Ag/AgCl electrode). The response speed of the abovementioned current path is dominated by the RC circuit formed by R_{S1} and C_{mb1}. R_{mb1} is not included in the estimation of response speed because R_{mb1} is a purely resistive path for ion current flow and hence the time-dependent current across basolateral membrane due to the sweeping of V_{TE} passes through C_{mb1} instead of R_{mb1}. Consider $R_{S1} = 10$ MΩ and $C_{mb1} = 30$ pF, the RC time constant can be calculated by the product of R_{S1} and C_{mb1}, which yields 0.3 ms. V_{TE} is swept at 1 Hz in P-SICM measurement and as such is much slower than the response speed of this RC circuit.

An alternative way to estimate the rate-dependent effect exerted on V_1' by sweeping V_{TE} is to calculate the potential change on V_1'. Initially before any potential is applied to WE, V_1 and V_1' are held at E_{rest}. As V_{TE} starts to change, a time-dependent current passes through C_{mb1} and this current (I) can be calculated from the fundamental description of a capacitor and **Equation 5** below.

$$\Delta V_{TE} \cdot C_{mb1} = I \cdot \Delta t \tag{5}$$

In **Equation 5**, the product of the capacitance and voltage difference across a capacitor equals the charge on the capacitor. In this case, changes in V_{TE} (ΔV_{TE}) during time Δt induce the voltage difference across C_{mb1} from the initial state, with I representing current through C_{mb1}. Rearrangement of **Equation 5** yields:

$$\frac{\Delta V_{TE}}{\Delta t} \cdot C_{mb1} = I \tag{6}$$

where $\frac{\Delta V_{TE}}{\Delta t}$ represents the sweeping rate of V_{TE}. As described previously, V_{TE} is swept from −50 mV to +50 mV at 1 Hz and therefore $\frac{\Delta V_{TE}}{\Delta t} = 0.2 V/s$. The current I is calculated to be 6 pA according to **Equation 6** if 30 pF is used for C_{mb1}. The current I then flows through R_{S1} to the amplifier and $V_1 = V_1'$ no longer holds. If $R_{S1} = 10$ MΩ, a 60 μV ($I \cdot R_{S1}$) voltage difference is induced by V_{TE} through the RC circuit, which is small enough to be compensated by patch clamp amplifier. One thing worth mentioning is that, the patch clamp amplifier response speed in controlling V_1 is not discussed because the frequency of V_{TE} is much smaller than the upper limit of signal frequency (tens to hundreds of kHz) accessible by most patch clamp amplifiers.

Conclusion

We have described an approach to isolate and measure paracellular ionic permeability, with minimal contributions from transcellular pathways. The approach is based on previous developments in potentiometric scanning ion conductance microscopy and voltage clamp methods. Ultimately, we expect the approach described here will lead to definitive measurements of ion permeation through tight junctions, especially at nanometer scales, and with the potential of identifying discrete conductance events of the paracellular ion channels. This new approach will allow revealing previously unknown aspects of the tight junction in physiological and pathophysiological processes.

Disclosure of Potential Conflicts of Interest

No potential conflicts of interest were disclosed.

Acknowledgment

We acknowledge Andy Alexander of Indiana University EIS for enlightening discussions.

Funding

This work is supported by grants from National Institute of Diabetes and Digestive and Kidney Diseases - RO1DK084059 and Department of Defense - HDTRA1-11-16-BRCWMD-BAA.

References

1. Farquhar MG, Palade GE. Junctional complexes in various epithelia. J Cell Biol 1963; 17, 375-412; http://dx.doi.org/10.1083/jcb.17.2.375
2. Goodenough DA, Revel, JP. A Fine structural analysis of intercellular junctions in the mouse liver. J Cell Biol 1970; 45:272-90; PMID:4105112; http://dx.doi.org/10.1083/jcb.45.2.272
3. Furuse M, Hirase T, Itoh M, Nagafuchi A, Yonemura S, Tsukita S, Tsukita S. Occludin: a novel integral membrane protein localizing at tight junctions. J Cell Biol 1993; 123:1777-88; PMID:8276896; http://dx.doi.org/10.1083/jcb.123.6.1777
4. Ebnet K, Suzuki A, Ohno S, Vestweber D. Junctional adhesion molecules (JAMs): more molecules with dual functions? J Cell Sci 2004; 117:19-29; PMID:14657270; http://dx.doi.org/10.1242/jcs.00930
5. Furuse M, Fujita K, Hiiragi T, Fujimoto K, TsuKita S. Claudin-1 and-2: novel integral membrane proteins localizing at tight junctions with no sequence similarity to occludin. J Cell Biol 1998; 141:1539-50; PMID:9647647; http://dx.doi.org/10.1083/jcb.141.7.1539
6. Alan S, Enck AH, Lencer WI, Schneeberger EE. Claudin-8 expression in Madin-Darby canine kidney cells augments the paracellular barrier to cation permeation. J Biol Chem 2003; 278:17350-9; PMID:12615928; http://dx.doi.org/10.1074/jbc.M213286200
7. Ben-Yosef T, Belyantseva IA, Saunders TL, Hughes ED, Kawamoto K, Van Itallie CM, Beyer LA, Halsey K, Gardner DJ, Wilcox ER, et al. Claudin 14 knockout mice, a model for autosomal recessive deafness DFNB29, are deaf due to cochlear hair cell degeneration. Hum Mol Genet 2003; 12:2049-61; PMID:12913076; http://dx.doi.org/10.1093/hmg/ddg210
8. Colegio OR, Van Itallie CM, McCrea HJ, Rahner C, Anderson JM. Claudins create charge-selective channels in the paracellular pathway between epithelial cells. Am J Physiol.: Cell Physiol 2002; 283:C142-7; PMID:12055082; http://dx.doi.org/10.1152/ajpcell.00038.2002
9. Van Itallie C, Rahner C, Anderson JM. Regulated expression of claudin-4 decreases paracellular conductance through a selective decrease in sodium permeability. J Clin Invest 2001; 107:1319; PMID:11375422; http://dx.doi.org/10.1172/JCI12464
10. Wen H, Watry DD, Marcondes MCG, Fox HS. Selective decrease in paracellular conductance of tight junctions: role of the first extracellular domain of claudin-5. Mol Cell Biol 2004; 24:8408-17; PMID:15367662; http://dx.doi.org/10.1128/MCB.24.19.8408-8417.2004
11. Van Itallie CM, Fanning AS, Anderson JM. Reversal of charge selectivity in cation or anion-selective epithelial lines by expression of different claudins. Am J Physiol Renal Physiol 2003; 285:F1078-1084; PMID:13129853; http://dx.doi.org/10.1152/ajprenal.00116.2003
12. Conrad MP, Piontek J, Gunzel D, Fromm M, Krug SM. Molecular basis of claudin-17 anion selectivity. Cell Mol Life Sci 2015; PMID:26194246
13. Tang VW, Goodenough DA. Paracellular ion channel at the tight junction. Biophys J 2003; 84:1660-73; PMID:12609869; http://dx.doi.org/10.1016/S0006-3495(03)74975-3
14. Van Itallie CM, Holmes J, Bridges A, Gookin JL, Coccaro MR, Proctor W, Colegio OR, Anderson JM. The density of small tight junction pores varies among cell types and is increased by expression of claudin-2. J Cell Sci 2008; 121:298-305; PMID:18198187; http://dx.doi.org/10.1242/jcs.021485
15. Saitoh Y, Suzuki H, Tani K, Nishikawa K, Irie K, Ogura Y, Tamura A, Tsukita S, Fujiyoshi Y. Structural insight into tight junction disassembly by Clostridium perfringens enterotoxin. Science 2015; 347:775-8; PMID:25678664; http://dx.doi.org/10.1126/science.1261833
16. Madara JL. Increases in guinea pig small intestinal transepithelial resistance induced by osmotic loads are accompanied by rapid alterations in absorptive-cell tight-junction structure. J Cell Biol 1983; 97:125-36; PMID:6863387; http://dx.doi.org/10.1083/jcb.97.1.125
17. Pappenheimer J. Physiological regulation of transepithelial impedance in the intestinal mucosa of rats and hamsters. J Membr Biol 1987; 100:137-48; PMID:3430570; http://dx.doi.org/10.1007/BF02209146
18. Ussing HH, Zerahn K. Active Transport of Sodium as the Source of Electric Current in the Short−circuited Isolated Frog Skin. Acta Physiol Scand 1951; 23:110-27; PMID:14868510; http://dx.doi.org/10.1111/j.1748-1716.1951.tb00800.x
19. Van Itallie C, Rahner C, Anderson JM. Regulated expression of claudin-4 decreases paracellular conductance through a selective decrease in sodium permeability. J Clin Invest 2001; 107:1319-27; PMID:11375422; http://dx.doi.org/10.1172/JCI12464
20. Hou J, Paul DL, Goodenough DA. Paracellin-1 and the modulation of ion selectivity of tight junctions. J Cell Sci 2005; 118:5109-18; PMID:16234325; http://dx.doi.org/10.1242/jcs.02631
21. Krug SM, Fromm M, Günzel D. Two-Path Impedance Spectroscopy for Measuring Paracellular and Transcellular Epithelial Resistance. Biophys. J 2009; 97:2202-11; PMID:19843452; http://dx.doi.org/10.1016/j.bpj.2009.08.003
22. Neher E, Sakmann B, Steinbach J. The extracellular patch clamp: A method for resolving currents through individual open channels in biological membranes. Pflügers Arch 1978; 375:219-28; PMID:567789; http://dx.doi.org/10.1007/BF00584247
23. Fromter E, Diamond J. Route of passive ion permeation in epithelia. Nat New Biol 1972; 235:13; http://dx.doi.org/10.1038/newbio235009a0
24. Higgins JT, Jr, Cesaro L, Gebler B, Frömter E. Electrical properties of Amphibian urinary bladder epithelia. Pflügers Arch 1975; 358:41-56; PMID:808794; http://dx.doi.org/10.1007/BF00584568
25. Hansma P, Drake B, Marti O, Gould S, Prater C. The scanning ion-conductance microscope. Science 1989; 243:641-3; PMID:2464851; http://dx.doi.org/10.1126/science.2464851
26. Chen CC, Zhou Y, Morris CA, Hou J, Baker LA. Scanning ion conductance microscopy measurement of paracellular channel conductance in tight junctions. Anal Chem 2013; 85:3621-8; PMID:23421780; http://dx.doi.org/10.1021/ac303441n
27. Cereijido M, Stefani E, Palomo AM. Occluding junctions in a cultured transporting epithelium: Structural and functional heterogeneity. J Membr Biol 1980; 53, 19-32; PMID:7373646; http://dx.doi.org/10.1007/BF01871169
28. Gitter AH, Bertog M, Schulzke JD, Fromm, M. Measurement of paracellular epithelial conductivity by conductance scanning. Pflügers Arch - Eur J Physiol 1997; 434:830-40; http://dx.doi.org/10.1007/s004240050472
29. Bindslev N, Tormey JM, Wright EM. The effects of electrical and osmotic gradients on lateral intercellular spaces and membrane conductance in a low resistance epithelium. J Membr Biol 1974; 19:357-80; PMID:4549221; http://dx.doi.org/10.1007/BF01869986
30. Reuss L. Electrical properties of the cellular transepithelial pathway inNecturus gallbladder: III. Ionic permeability of the basolateral cell membrane. J Membr Biol 1979; 47:239-59; PMID:480334; http://dx.doi.org/10.1007/BF01869080
31. Zhou Y, Chen CC, Weber AE, Zhou L, Baker LA. Potentiometric-scanning ion conductance microscopy. Langmuir 2014; 30:5669-75; PMID:24773406; http://dx.doi.org/10.1021/la500911w
32. Churchill D, Caveney S. Double whole-cell patch-clamp characterization of gap junctional channels in isolated insect epidermal cell pairs. J Membr Biol 1993; 135:165-80; PMID:8411137; http://dx.doi.org/10.1007/BF00231442
33. Neyton J, Trautmann A. Single-channel currents of an intercellular junction. Nature 1985; 317:331-5; PMID:2413362; http://dx.doi.org/10.1038/317331a0
34. Newman J. Resistance for Flow of Current to a Disk. J Electrochem Soc 1966; 113:501-2; http://dx.doi.org/10.1149/1.2424003
35. Hodgkin AL, Huxley AF. Action potentials recorded from inside a nerve fibre. Nature 1939; 144:710-1; http://dx.doi.org/10.1038/144710a0
36. Hodgkin AL, Huxley AF. A quantitative description of membrane current and its application to conduction and excitation in nerve. J Physiol 1952; 117:500-44; PMID:12991237; http://dx.doi.org/10.1113/jphysiol.1952.sp004764
37. Hodgkin AL, Katz B. The effect of sodium ions on the electrical activity of the giant axon of the squid. J Physiol 1949; 108:37-77; PMID:18128147; http://dx.doi.org/10.1113/jphysiol.1949.sp004310
38. Keynes R. The kinetics of voltage-gated ion channels. Q Rev Biophys 1994; 27:339-434; PMID:7540309; http://dx.doi.org/10.1017/S0033583500003097
39. Rook M, Jongsma H, Van Ginneken A. Properties of single gap junctional channels between isolated neonatal rat heart cells. Am J Physiol: Heart Circ Physiol 1988; 255:H770-82
40. Joyner RW, Sugiura H, Tan RC. Unidirectional block between isolated rabbit ventricular cells coupled by a variable resistance. Biophys J 1991; 60:1038; PMID:1760503; http://dx.doi.org/10.1016/S0006-3495(91)82141-5
41. Kameyama M. Electrical coupling between ventricular paired cells isolated from guinea−pig heart. J Physiol 1983; 336:345-57; PMID:6875911; http://dx.doi.org/10.1113/jphysiol.1983.sp014585
42. Kumar R, Wilders R, Joyner RW, Jongsma HJ, Verheijck EE, Golod DA, van Ginneken AC, Goolsby WN. Experimental model for an ectopic focus coupled to ventricular cells. Circulation 1996; 94:833-41; PMID:8772708; http://dx.doi.org/10.1161/01.CIR.94.4.833